Terra Antartica
2001, 8(4), 569-582

Sand Provenance from Major and Trace Element Analyses of Bulk Rock and Sand Grains from CRP2/2A, Victoria Land Basin, Antarctica

P. ARMIENTI[1*], M. TAMPONI[1] & M. POMPILIO[2]

[1]Dipartimento di Scienze della Terra, Università di Pisa, Via S. Maria 53, I-56126 Pisa - Italy
[2]Istituto Nazionale di Geofisica e Vulcanologia, Piazza Roma 2, I-95123 Catania - Italy

Received 7 June 2001; *accepted in revised form* 30 November 2001

Abstract - Sixty-four volcanic clasts, sandstones and tephras between 5.95 and 618.19 meters below sea floor (mbsf) in the Cape Roberts Project cores 2 and 2A cores (CRP-2/2A) were examined for Cenozoic and Mesozoic volcanic components, using optical and Scanning Electron Microscopy. Minerals and glass shards in a selection of samples were analysed by electron microprobe fitted with an EDAX detector. Laser-Ablation ICP-Mass-Spectrometry (ICP-MS) was used to determine rare earth elements and 14 additional trace elements in glass shards, pyroxenes and feldspars in order to pin-point the onset of McMurdo Volcanic Group (MVG) activity in the stratigraphic column. Pumices in tephra layers of peralkaline phonolite composition in Unit 7.2 -between 108 and 114 mbsf - were also analysed for trace elements by ICP-MS. This tephra unit is not reworked and its isotopic age (21.44 ± 0.05 Ma) is the age of deposition. The height of the eruptive column responsible for the deposition of the tephra was probably less than 8 km; the source was local, probably within 30 km from the drill site. Phonolite of unit 7.2 of CRP-2/2A has no direct petrogenetic relation with the peralkaline trachyte in the tephra-enriched layer of CRP-1 at 116.55 mbsf.

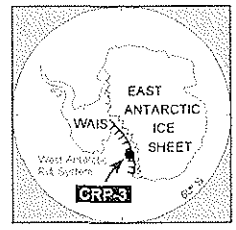

Volcanic clasts and sand grains (glass shards, aegirine-augite, anorthoclase) related to Cenozoic activity of MVG were observed only starting from Unit 9.8, where they are dated at 24.22 ± 0.06 Ma at *c.* 280 mbsf. In this unit the lowest- occurring basaltic glass shard is found at 297.54 mbsf. Sampled McMurdo volcanics are generally vesicular and vary in composition from alkali basalt to trachyte and peralkaline phonolite. By contrast, below 320 mbsf, aphyric or slightly-porphyritic volcanic clasts become more abundant but they are all non-vesiculated, pigeonite and ilmenite-bearing basalts and dolerite of tholeiitic affinity. These rocks are considered to be related to lava flows and associated intrusions of Jurassic age (Kirkpatrick basalts and Ferrar dolerite).

As in CRP-1, McMurdo volcanics appear to derive from a variety of lithologies. Besides glaciers, a dominant role of wind transportation from exposed volcanic rocks may be inferred from the contemporary occurrence of glass shards of different compositions at depths above 297.54 mbsf. These data confirm that the onset of magmatic activity in southern Victoria Land is considerably delayed (by about 24 Ma) with respect to northern Victoria Land.

INTRODUCTION

Most of the samples examined in this study range in age from Quaternary to Early Oligocene. In Early Cenozoic, Victoria Land suffered a considerable uplift-denudation period (Balestrieri et al., 1997), during which erosion of alkaline volcanoes of the McMurdo Volcanic Group started to supply volcaniclastic components to the sedimentary basin of the Ross Sea. Moreover the effects of persistent glaciers on the East Antarctic craton appear at the Eocene/Oligocene boundary (Ehrmann & Mackensen, 1992; Diester-Haass et al., 1996) thus providing a complex framework for interpretation of the sedimentary record of CRP-2/2A. Previous results obtained at the nearby CRP-1 drillsite indicate that the supply of volcanic particles is mainly due to the effect of winds that spread loose volcanic detritus from exposed areas, over local glaciers or on sea ice, from where they reached the sedimentation site. At CRP-1 the only evidence of tephra linked to an eruption is found at 116.55 mbsf where a thin layer of pumice fragments of trachyte composition occurs (Armienti et al., 1998). Distinctly higher amounts of McMurdo volcanic components are recorded at CRP-1 above 62 mbsf, in layers overlapping in age with the volcanic activity in the McMurdo Sound.

PETROGRAPHIC DATA

Smellie (2000) described textural and modal data for sandstones and fine sandstones of 30 samples examined in this work. In addition we determined the petrographic composition of 34 volcanic clasts of alkaline and tholeiitic affinity (Tab. 1). A wide variety

*Corresponding author (armienti@dst.unipi.it)

of glass shards was also analysed in the sand fraction at depths above 297.54 mbsf.

MCMURDO VOLCANIC GROUP CLASTS AND SAND GRAINS ABOVE 297.54 mbsf.

Although Ferrar dolerite clasts occur throughout the whole core (Talarico et al., 2000), volcanic clasts and grains of the McMurdo Volcanic Group are only found within and above Unit 9.8. They derive from alkaline magmas and are readily recognised by the occurrence of olivine in the groundmass of mafic lavas and the attainment of peralkaline composition in evolved rocks; size of clasts varies from 1 to 5 cm. Bulk sediments enriched in tephra and hand-picked pumice fragments were also collected throughout Unit 7.2 (see below), at 193.45 (Unit 9.2) and at 280.10 mbsf (Unit 9.8; the lowermost occurrence of glass shards large enough to analyse). The pumices are highly vesiculated and almost crystal free. Tephra found in Unit 9.8 was dated at 24.22 ± 0.06 Ma (Cape Roberts Science Team, 1999).

Petrographical examination of McMurdo Volcanic Group (MVG) clasts reveals the occurrence of lavas varying in composition from alkali basalt to trachyte, but alkali basalt and hawaiite are most common. Alkali basalt clast CRP-2/2A 203.75 mbsf is characterised by the presence of olivine phenocrysts, completely altered to bowlingite, and bytownitic plagioclase microphenocrysts. This clast also contains partly resorbed xenocrysts of quartz with a clinopyroxene reaction rim, a textural feature that is commonly observed in MVG basic rocks (Armienti et al., 1991). The complete alteration of olivine in this sample may account for the scarcity of olivine sand grains in CRP-1 and CRP-2/2A sediments (Smellie, 1998, 2000). Clasts of hawaiite and mugearite lavas mostly have fluidal textures with plagioclase and augite phenocrysts. The optically determined composition of plagioclase (labradorite) matches that of crystals supplied from MVG to the sand fraction of CRP-1 (Armienti et al., 1998). One basaltic clast (CRP-2/2A 122.82 mbsf) shows an outer rim of tachylitic glass with small plagioclase microcrysts. The rim is closely comparable to opaque fragments found in the uppermost 300 m of CRP-2/2A and throughout CRP-1 (Cape Roberts Science Team, 1998, p. 47, Fig. 12-f). Felsic clasts (trachyte and syenite) differ in the degree of crystallinity: they are characterised by the occurrence of sanidine and/or anorthoclase microphenocrysts, commonly accompanied by zoned green aegirine-augite microphenocrysts; fayalitic olivine also occurs in the syenite clast in CRP-2/2A at 258.88 mbsf.

Parts of the sequence are rich in volcanic components (*e.g.* Unit 7.2, Unit 9.2 at 193.45 mbsf and Unit 9.8 *c.* 280 mbsf). They contain abundant fresh, crystal-poor glass that is commonly highly

Tab. 1 - Petrographic description of CRP-2/2A samples discussed in this paper.

DEPTH [mbsf]	Petrographic description
	DEPTH < 300 mbsf
36.01	Trachyte clast consisting of glassy matrix with plagioclase and sanidine microphenocrysts.
43.75	Layer enriched in phonolitic pumices. Brown glass of intermediate composition is also present.
78.76	Isolated clast of alkali basalt scoria.
79.07	Basanite fragment with olivine microcrysts. Plagioclase in the groundmass.
97.26	Crystal-free lapillistone.
111.73	Lapillistone made of crystal free phonolitic pumices.
112.25	Lapillistone made of crystal free phonolitic pumices.
113.75	Lapillistone. Reworked layer with abundant pumices and quartz-feldspar sand grains.
114.08	Lapillistone made of crystal free phonolitic pumices.
122.06	Poorly porphiritic clast of trachyte. Plagioclase phenocrysts and magnetite microphenocrysts are present. Sanidine occurs in the groundmass.
122.82	Two basaltic clasts are present: the first is an oxide-bearing tachylitic glass; the second consists of brown basaltic glass with plagioclase and olivine microphenocrysts.
132.06	Isolated clast of partially devitrified trachytic scoria.
141.39	Diamictite with a clast of trachytic lava with plagioclase microphenocrysts and quench crystals of sanidine. Rare augite microphenocrysts. The silt matrix contains small fragments of basaltic glass.
143.05	Aphyric basaltic scoria and two fragments of aphyric trachytic pumices. Abundant tephra fragments occur in the sedimentary matrix.
143.16	Pumices, tachylitic glasses and rare basalt glass shards.
187.44	Trachyte clast.
193.45	Sandstone with basaltic scoriae and pumice fragments.
203.75	Rounded clast of devitrified alkali basalt. The clast contains olivine phenocrysts altered to iddingsite and rounded quartz xenocrysts. Scarce plagioclase microphenocrysts are also present. The silt matrix is characterized by the widespread occurrence of basaltic glass.
203.86	Fine sandstone with clay matrix. In the fine fraction glass shards of basaltic to intermediate composition are also present.
209.40	Coal grain in a sandstone matrix. No glass.
221.90	Sandstone composed by basaltic and tachylitic glass shards. Dolerite fragments are also present.
221.91	Sandstone. No glass shards in the matrix. Dolerite fragments are present.
227.63	Basement clasts. No glass shard in the sandstone matrix.
252.73	Abundant fragments of basaltic glass, isolated aegirine crystals, trachytic microcrystalline lava clasts with interstitial aegirine.
258.88	Siltstone. Rare trachyte grains and isolated aegirine crystals.
259.60	Siltstone. No glass shards.
262.32	Siltstone. Rare vesiculated fragments of basaltic glass.
264.12	Diamictite. No glass fragment in the sand matrix.
280.06	Sandstone. Layer enriched to phonolitic pumice fragments and basaltic glass shards. The volcanic material is reworked.
295.19	Sandstone, scarce, altered basaltic glass and abundant carbonate cement.
297.54	Sporadic basaltic glass in the silt matrix.
	DEPTH >300 mbsf
324.38	Rounded grain of Kirkpatrick basalt showing a holocrystalline texture with needle-shaped crystals of plagioclase. Microfragments of pyroxene crystals together with radial intergrowths of augite and plagioclase.
324.93	Diamictite. Silt matrix containing two dolerite clasts, characterized by interstitial amphibole.
326.29	Diamictite. No glass shards in the matrix. Dolerite fragments are present.
349.02	Subophytic dolerite clast with interstitial glass.
353.67	Diamictite with dolerite clasts, ilmenite-bearing basalt and rounded quartz grains. No glass in the sand matrix.
372.05	Subophytic dolerite. No fresh glass in the matrix. Tachylitic fragments and coal are also present.
388.34	Subophitic dolerite.
388.57	Dolerite clast.
408.11	Subophitic dolerite and basalt showing quench texture Plagioclase and ilmenite crystals occur with intersertal glass. No glass shards in the sedimentary matrix.
439.27	Coal fragments. No glass shards in the sedimentary matrix.
488.01	Kirkpatrick basalt and amphibole-bearing dolerites.
518.95	Kirkpatrick basalt containing dolerite xenoliths and quartz xenocrysts. Vesicles show epidote rims.
572.95	Quartz-bearing dolerites. Carbonate cement is present.
618.19	Dolerite clast.
619.29	Fine grained, hypocrystalline clast of Kirkpatrick basalt. No glass shards in the sedimentary matrix.

vesiculated pumice; glass is generally associated with grains of a wide variety of volcanic rocks. No level was found to be as rich in basaltic glass shards as the CRP-1 Lower Miocene sediments at 43.62 mbsf and at around 60 mbsf (Armienti et al., 1998). The sandstone matrix of the diamictite above 280.10 mbsf contains a variety of basalt to trachyte glass shards although basaltic compositions are most common. In the matrix, minor amounts of green (Mg-hornblende) to brown hornblende (kaersutite), pink titaniferous augite and aegirine are ubiquitous. Sporadic grains of kaersutite, aenigmatite and arfvedsonite are present in samples in which evolved glasses are more abundant, and these are often associated with anorthoclase crystals. Micas (muscovite and biotite) and opaque minerals (Ti-magnetite, ilmenite and sulphides) are not abundant, and they represent an almost constant fraction of less than 1% of the grains. Apatite, zircon, pink garnet and monazite are found among accessory grains.

TEPHRA LAYERS OF UNIT 7.2 (108 - 114 mbsf)

Special attention was devoted to Unit 7.2 that contains seven main layers of tephra (Fig. 1). The tephra layer provided $^{40}Ar/^{39}Ar$ age of 21.44 ± 0.05 Ma (McIntosh, Cape Roberts Science Team, 1999). Larger pumices from different layers were also hand-picked for whole-rock chemical analyses to establish any compositional variation. Tephras are scattered throughout Unit 7.2; thin beds of fine sandstone and siltstone separate discrete pumice-rich beds. Some beds have dispersed pumice whose modal fraction is very variable. Many of the pumice lapilli, including pumice in the thicker layer (1.2 m), are well rounded. The 1.2 m-thick layer and the layer at the bottom of the unit (*c.* 114 mbsf; Fig. 1) contain a high proportion of fine glassy tuff matrix. Sample CRP-2/2A-111.28 mbsf is a poorly bedded, poorly sorted lapillistone, with a 5% mix of lithic clasts and medium- fine sand matrix, supporting pumice lapilli

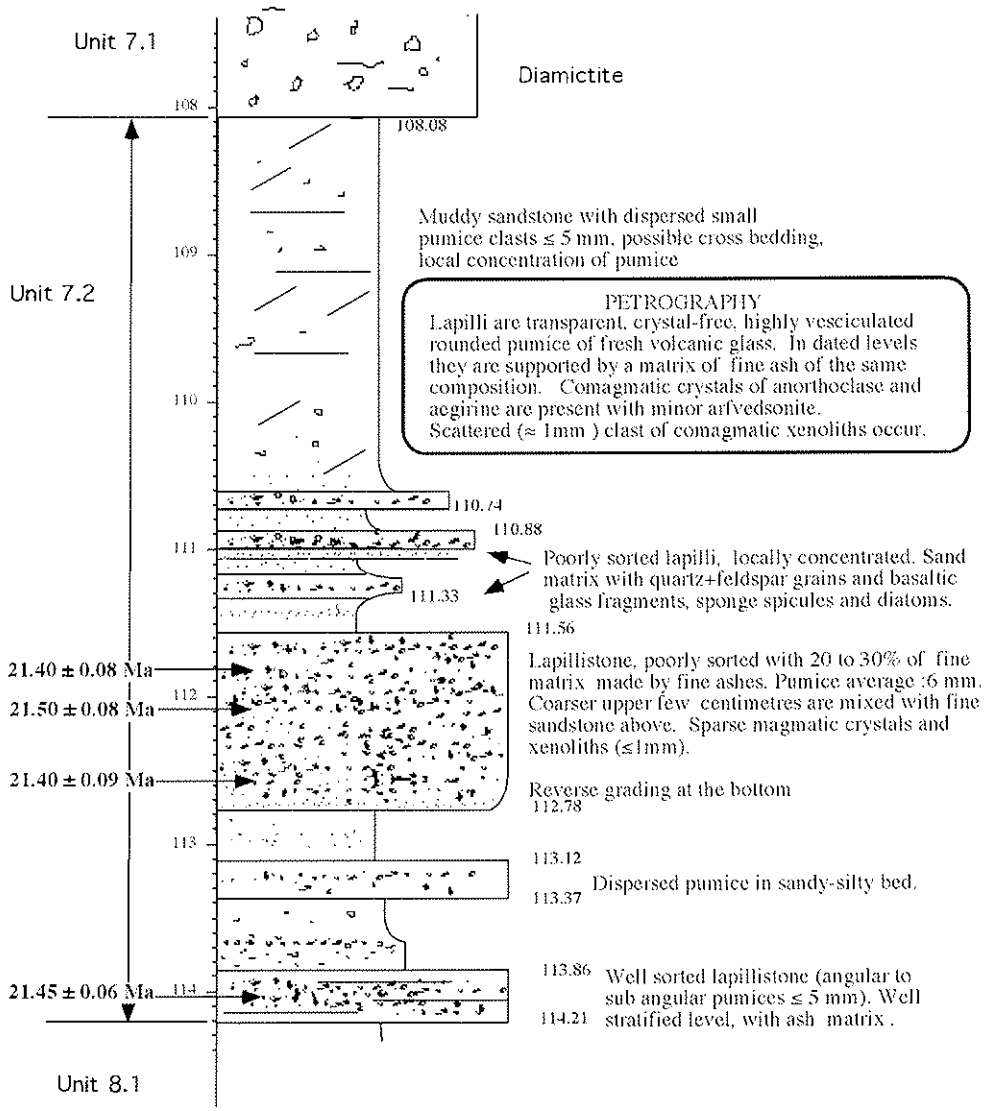

Fig. 1 - Stratigraphic log of ash-rich Unit 7.2, with petrographical and geochronological information ($^{40}Ar/^{39}Ar$ dating: from Cape Roberts Science Team, 1999).

ranging in size from about 10 mm to less than 1 mm. The pumices consist of highly vesiculated colourless glass. The matrix consists of quartz and feldspar fragments with abundant brown glass shards, green hornblende and pyroxene. Sponge spicules and diatoms are common. Samples CRP-2/2A-111.77, and -112.25 mbsf (from the 1.2 m-thick layer) and CRP-2/2A-114.12 mbsf (from the 0.35 m thick layer at the base of Unit 7.2) come from beds of tephra dominated by poorly sorted pumice of lapilli size (70-80%) set in a matrix of very fine grained volcanic ash. The high proportion of ash matrix is possibly due to the high vesiculation and corresponding buoyancy of the pumice that made it sink as slowly as the ash. Lapilli are almost crystal-free, highly vesiculated and colourless pumice. These deposits also contain scattered crystals of alkali feldspar, aegirine-augite and sporadic Na-amphibole (arfvedsonite). Small fragments (<1 mm) of altered volcanic rocks, holocrystalline trachyte and sporadic angular quartz are probably derived from the basement of the volcano and were incorporated during explosive activity. The paucity of comagmatic plagioclase feldspar, the occurrence of anorthoclase, aegirine-augite and arfvedsonite indicate a peralkaline composition for the juvenile magma. In these two beds, the absence of detrital sand grains, that would occur within the matrix if the layer had suffered re-deposition within the basin, suggests that the two layers represented by CRP-2/2A-111.77, 112.25 and 114.12 are probably derived by direct sinking of sub-aerial falls of tephra. Preservation of delicate grading within these ash-rich tephra layers also argues against redeposition. Some subdivisions proposed on the basis of grading and grain size variations in the 1:20 core log could be simply linked to different settling velocities of larger particles in the water column, rather than pulsing eruptive activity. The rounded shapes of many lapilli suggest that they may have spent some time within floating rafts prior to sinking. The very top of the 1.2 m-thick bed contains small pockets of silt-size crystals + brown glass, thus offering direct evidence of the effects of minor reworking that may have occurred at the upper limit of the layer.

VOLCANIC CLASTS BELOW 297.54 mbsf

Dolerite and basalt samples become frequent in the core below 300 mbsf. They range from sand size fragments to boulders but are characterised by the widespread occurrence of sub-calcic pyroxene and ilmenite, thus related to the Mesozoic tholeiitic magmatic activity. Table 1 reports summary descriptions of the samples examined. Clasts are usually holocrystalline with ophitic to sub-ophitic intergrowths of plagioclase and augite; sub-ophitic varieties are usually fine grained with felted intergrowths of plagioclase and augite. Some hypocrystalline samples contain intersertal oxidised tachylite and microphenocrysts of plagioclase and pyroxene; none of this basaltic rocks is vesiculated. Interstitial ilmenite and magnetite are ubiquitous together with sub-calcic pyroxene. Some samples contain magnetite phenocrysts. Olivine phenocrysts are rare and show resorption or reaction rims. A careful investigation of the sandy matrix enclosing the clasts revealed no alkaline glass shards or alkaline minerals, which are commonly found in the upper part of the core. Black fragments reported in the core log are coal and/or dolerite fragments. Some sand size volcanic fragments are oxidised tachylites and contain plagioclase microlites and resemble the groundmasses of hypocrystalline Kirkpatrick basalts.

ANALYTICAL METHODS

Major element mineral chemistry of selected samples was determined at Pisa University using an energy-dispersive analyser (EDAX PV 9900) mounted on a Philips XL30 Scanning Electron Microscope, using the software EDAX DX4 2.11 that allows microanalytical determinations to be made without external reference standards and ensures faster acquisition of data. This method, however, recalculates analyses to 100%. Calibration was obtained by using 29 international standards of minerals and glasses, according to the procedure of Leoni et al. (1989). Results obtained showed, for major elements, precision and accuracy comparable to those yielded by wavelength dispersive microprobe analyses. Mean percentile errors, with few exceptions, are between 2% and 4% for absolute concentrations of about 3 wt%, and between 0.5% and 2% for absolute concentrations larger than 10 wt%. Detection limits range from 0.08 wt% (Fe) to 0.15 wt% (Na). Microanalyses were performed on polished carbon-coated thin sections. Instrumental conditions were: acceleration voltage: 20 kv, tilt angle 0°, take-off angle 35.16°, counting time 100s with about 2700 counts per second, electronic beam diameter 0.2-0.5 μm, and window thickness 0.3 μm. Matrix effect correction (ZAF) was obtained using the algorithms of Philibert (1963) and Duncumb & Reed (1968). To minimise alkali loss, glass grains were analysed with a defocused beam or in «window» mode. In spite of this, the strong vesiculation and very high alkali content of more evolved glass shards induced some mobilisation of Na causing analytical artifacts such as normative Corundum in the CIPW norm. All peraluminous trachyte analyses were thus discarded from the data set.

Glasses and minerals were analysed for trace elements at the C.N.R.-CSG laboratory in Pavia (Italy), by laser-ablation microprobe-inductively coupled plasma-mass spectrometry (LAM-ICP-MS) using a UV (266 nm) laser probe developed at the

Memorial University of Newfoundland, Canada (Jackson et al., 1992) and an "Element" (Finnigan MAT) mass spectrometer. Data were reduced using the software "LAMTRACE" by S. Jackson, according to the analytical protocol developed at Memorial University. Spot diameter varied from 25 μm to 80 μm; the analysed grains were always larger than 200 μm.

Hand-picked pumice fragments from Unit 7.2 were washed with bi-distilled water, then analysed by ICP-MS to determine concentrations of Sc, V, Cr, Co, Ni, Rb, Sr, Y, Zr, Nb, Cs, Ba, REE, Hf, Ta, Pb, Th and U. Powdered pumices were dissolved by conventional HNO_3+HF acid digestion, then spiked with Rh, Re and Bi (internal standards). Analytical precision, estimated by repeated analyses of geochemical reference samples, typically ranges from about 10% at 10x detection limit, to 3-5% at 100x detection limit; consequently different numbers of significant digits are used to report results. The accuracy of data, evaluated by regularly analysing well-certified geochemical reference samples, typically ranges from 0 to 7% for elements at 50 -100X detection limit.

GEOCHEMISTRY OF GLASS SHARDS: MAJOR AND TRACE ELEMENTS

Glass fragments provide a quick and reliable key to detect the occurrence and recognise the variability of alkaline magmas in the sedimentary sequence (Armienti et al., 1998). They are usually easily recognised due to vesiculation, and careful SEM inspection can find traces of glass when only a small amount is present. Tables 2 and 3 report selected glass analyses for major and trace elements, respectively, measured with SEM-EDAX and ICP-MS. The first four analyses of table 3 are ICP-MS determinations of hand picked pumice fragments from the tephra Unit 7.2, and may be compared to LAM-ICP-MS analyses on isolated fragments at the corresponding depths. Most evolved alkali-rich samples of phonolitic composition are highly vesiculated and can only be analysed with finely collimated beams. This often causes Na diffusion in the areas exposed to the electron beam and can lead to under-determination of Na, producing peraluminous compositions when recast for CIPW norms. Some alkali loss cannot be excluded for the most alkaline pumice fragments and can be partly responsible for the scatter of analyses, in the TAS diagram of figure 2, of otherwise similar fragments from the same depth. The variable composition (alkali basalt to phonolite, Tab. 2, Fig. 2) found in glass shards of the sample from 111.13 mbsf confirms the occurrence of reworking in the upper part of tephra-rich unit 7.2. Other samples from the tephra -rich layers of unit 7.2 are compositionally more uniform. Pumices from the levels from 280.30 and 280.06 mbsf, range in composition from mugearite to phonolite and trachyte.

Compositional variability of the analysed fragments overlaps the compositional spectrum of McMurdo volcanism, including transitional, mildly alkaline and alkaline volcanics (Fig. 2). A hiatus is evident in the data set and is distinctive of MVG volcanic activity (Armienti et al, 1991). The most-evolved lavas attain a peralkaline composition, and phonolitic pumice of the tephra layer is very alkali-rich (Na_2O=10%, K_2O=5%), attaining the compositions of extremely differentiated phonolites of

Tab. 2 - Selected major element compositions of glass shards and pumice from CRP-2/2A. Analyses by SEM-EDS.

Depth	43.75	43.75	43.75	111.13	111.13	111.13	111.13	111.24	111.73	111.73	112.25	112.25	112.74	114.08	114.08
Label	shard	shard	shard	shard	shard	shard	shard	pumice	shard	shard	pumice	pumice	pumice	pumice	shard
SiO_2	60.45	61.16	62.82	46.87	47.42	58.03	63.43	55.35	54.90	54.44	53.99	53.53	53.08	52.63	52.17
TiO_2	0.22	0.28	0.59	4.40	2.86	0.05	0.39	1.59	1.67	1.75	1.84	1.92	2.00	2.08	2.17
Al_2O_3	19.00	18.98	16.52	13.92	16.32	20.24	14.96	15.73	15.38	15.03	14.68	14.33	13.98	13.63	13.28
FeO	4.71	5.05	5.45	12.24	8.52	3.86	7.66	8.15	8.49	8.83	9.17	9.51	9.85	10.19	10.53
MnO	<d.l.	<d.l.	<d.l.	0.38	0.19	0.17	0.36	0.47	<d.l.	<d.l.	<d.l.	<d.l.	0.57	0.24	<d.l.
MgO	0.38	0.31	0.28	5.52	6.96	0.12	0.37	2.43	0.06	0.13	0.39	0.26	0.31	0.24	0.31
CaO	1.50	1.59	1.16	10.40	12.74	0.72	1.18	5.28	0.90	0.92	0.79	0.71	0.78	0.99	0.82
Na_2O	7.17	5.97	7.49	3.93	3.32	10.94	6.38	6.01	10.14	8.56	10.37	10.15	8.63	9.10	7.89
K_2O	6.32	6.34	5.22	1.51	1.35	5.08	4.81	2.61	5.55	5.56	5.17	5.00	5.47	5.72	5.80
P_2O_5	<d.l.	<d.l.	<d.l.	0.69	0.24	0.18	<d.l.	0.43	<d.l.	<d.l.	<d.l.	<d.l.	<d.l.	<d.l.	<d.l.
Cl	0.25	0.32	0.47	0.14	0.08	0.61	0.46	<d.l.	0.65	0.69	0.57	0.52	0.62	0.65	0.71
	Phonolite	Trachyte	com.Trachyte	Hawaiite	Alk-bas.	Phonolite	com.Trachyte	Benmoreite	Phonolite	Phonolite	Phonolite	Phonolite	Phonolite	Phonolite	Phonolite

Depth	122.22	122.22	122.22	132.06	132.06	143.05	143.05	143.05	143.05	143.05	193.45	193.45	280.06	280.30
Label	shard	shard	shard	shard	shard	pumice	pumice	pumice	shard	pumice	shard	shard	shard	shard
SiO_2	44.77	45.31	47.68	59.86	63.39	47.09	48.47	59.14	63.99	62.33	44.35	49.22	64.24	67.45
TiO_2	5.26	5.05	2.64	<d.l.	0.66	3.60	3.46	0.21	0.22	0.46	4.6	2.34	0.58	0.71
Al_2O_3	13.09	13.23	16.05	19.73	14.01	15.47	14.86	19.25	16.70	16.77	14.55	15.97	14.94	10.03
FeO	15.31	15.58	10.21	4.38	9.30	10.40	12.66	4.64	5.42	5.76	12.33	8.68	6.13	9.82
MnO	0.43	0.21	0.12	0.29	0.39	0.06	0.37	0.41	0.12	0.16	0.36	<d.l.	0.56	0.37
MgO	4.95	4.69	6.96	0.24	0.61	6.26	4.31	0.42	0.57	0.36	6.11	7.41	0.67	0.06
CaO	10.33	10.20	11.84	0.80	2.00	11.61	8.30	0.96	0.92	1.00	10.35	12.17	1.14	0.67
Na_2O	3.78	3.82	3.21	8.39	4.70	3.44	4.85	8.83	6.36	6.59	3.66	3.09	6.27	6.26
K_2O	1.33	1.27	1.01	5.39	4.70	1.35	1.54	5.56	5.30	6.18	1.13	1.50	5.24	4.63
P_2O_5	0.62	0.50	0.28	0.26	<d.l.	0.67	1.08	<d.l.	<d.l.	0.00	<d.l.	<d.l.	<d.l.	<d.l.
S	0.07	0.07	<d.l.	0.03	<d.l.	0.05	0.06	0.04	<d.l.	0.02	<d.l.	<d.l.	<d.l.	<d.l.
Cl	0.06	0.07	<d.l.	0.63	0.24	<d.l.	0.04	0.54	<d.l.	0.37	<d.l.	<d.l.	<d.l.	<d.l.
	Tephrite	Hawaiite	Alk-bas.	Phonolite	Trachyte	Alk-bas.	Hawaiite	Phonolite	Trachyte	com.Trachyte	Tephrite	Alk. Basalt	com.Trachyte	pant.Trachyte

Tab. 3 - LAM-ICP-MS and conventional ICP-MS analyses of hand-picked pumices and selected glass shards from CRP-2/2A.

Depth	100.97	112.20	111.50	111.20	111.24	111.24	111.24	111.24	111.24	111.24	111.24
SiO_2					58.60 Trachyte	61.13 Trachyte	58.26 Trachyte	58.77 Trachyte	59.52 Trachyte	55.54 Benmoreite	59.66 Trachyte
Trace elements	ICP	ICP	ICP	ICP	LAM-ICP	LAM-ICP	LAM-ICP	LAM-ICP	LAM-ICP	LAM-ICP	LAM-ICP
Be	10.2	14.4	14.7	14.3							
Sc	9.1	5.3	5.4	5.4	2	4	4	4	4	11	3
V	31.9	< d.l.	3.0	3.0	<4	<4	<5	<7	3	43	<2
Cr	52.1	5.2	8.7	5.5	<25	<24	<36	<54	19	<29	14
Co	4.2	< d.l.	2.9	1.7							
Ni	24.6	3.5	5.5	4.3							
Rb	183.5	191.0	204.6	193.6	257	276	291	257	332	79	312
Sr	163.0	24.4	26.4	37.9	17	37	21	23	17	586	19
Y	89.5	123.2	120.4	120.3	111	122	128	134	126	44	124
Zr	1313.7	1853.5	1808.7	1813.9	2093	2107	2269	2200	2414	416	2290
Nb	280.1	395.2	386.8	386.4	406	445	443	440	457	90	451
Cs	3.4	3.4	3.7	3.5	4	5	5	5	5	1	4
Ba	231.4	10.2	11.9	26.4	5	10	9	5	7	1084	5
La	164.9	222.8	219.7	215.2	248	260	297	285	282	74	280
Ce	312.0	432.6	427.7	420.1	426	470	507	475	489	142	479
Pr	29.0	39.5	39.0	38.3	37	39	42	42	40	15	40
Nd	91.8	123.6	121.3	121.0	130	136	155	151	138	70	142
Sm	16.0	21.2	20.9	20.6	22	24	26	26	24	13	24
Eu	1.1	0.9	0.9	1.0	1	1	1	1	1	5	1
Gd	12.3	16.1	15.7	16.2	20	20	21	22	20	10	20
Tb	2.4	3.3	3.2	3.3	3	3	4	3	3	1	4
Dy	15.1	20.4	19.8	19.7	21	23	24	24	23	10	24
Ho	3.0	4.2	4.1	4.2	4	4	5	5	4	2	4
Er	8.7	12.0	11.5	11.6	12	12	12	14	12	4	13
Tm	1.3	1.7	1.7	1.8	2	2	2	2	2	1	2
Yb	7.6	10.6	10.3	10.4	11	13	15	14	13	4	14
Lu	1.1	1.5	1.5	1.5	2	2	2	2	2	0	2
Hf	27.1	38.8	37.4	37.7	40	44	48	47	45	8	47
Ta	17.0	24.5	23.7	23.8	19	22	23	23	22	5	22
Tl	1.1	1.0	1.3	0.7							
Pb	26.5	29.1	27.8	28.7	38	37	68	48	49	4	39
Th	24.1	32.2	32.2	31.5	32	34	36	37	34	7	36
U	7.1	9.7	9.8	9.7	10	11	13	11	11	2	12

Depth	111.28	111.28	112.47	112.47	112.74	112.74	112.74	122.22	122.22	122.22	132.06
SiO_2	61.37 Trachyte	55.74 Tephriphonolite	57.23 Phonolite	54.00 Tephriphonolite	57.51 Trachyte	59.77 Phonolite	61.57 Trachyte	45.08 Tephrite	47.07 alk Basalt	47.24 alk Basalt	62.51 Trachyte
Trace elements	LAM-ICP	LAM-ICP	LAM-ICP	LAM-ICP	LAM-ICP	LAM-ICP	LAM-ICP	LAM-ICP	LAM-ICP	LAM-ICP	LAM-ICP
Be											
Sc			3	3	<2	5	4				
V	5	5	4	4	<5	<8	3	33	19	19	9
Cr	5	5	<16	<15	<33	<43	<19	498	119	154	1
Co	21	9						<8	210	98	<10
Ni											
Rb	258	222	265	291	313	303	340	23	13	19	96
Sr	13	48	15	17	24	11	21	519	140	303	101
Y	103	102	109	113	122	127	124	28	4	14	72
Zr	1922	1800	2172	2110	2205	2235	2367	222	222	108	990
Nb	363	378	396	432	472	438	453	46	71	24	180
Cs	4	4	4	4	5	4	5	0	0	0	1
Ba	4	4	5	6	7	<5	5	336	18	35	590
La	235	226	262	251	273	271	272	38	4	20	130
Ce	394	381	451	451	460	454	470	78	9	42	259
Pr	34	31	37	37	39	40	40	9	1	5	25
Nd	107	86	127	129	140	138	140	36	3	16	81
Sm	16	14	21	23	27	25	25	7	1	3	15
Eu	1	1	1	1	1	1	1	3	0	1	3
Gd	17	13	17	18	18	21	19	7	1	4	16
Tb	3	3	3	3	3	4	3	1	0	1	3
Dy	21	18	19	19	21	23	22	7	1	4	16
Ho	4	4	4	4	4	4	4	1	0	1	3
Er	11	10	12	12	12	12	12	4	1	2	8
Tm	1	1	1	1	2	2	2	0	0	0	1
Yb	11	10	12	13	14	13	13	3	2	2	8
Lu	1	1	1	1	2	2	2	0	0	0	1
Hf	40	37	39	38	45	50	45	6	4	3	22
Ta	18	17	19	19	22	24	22	3	2	1	9
Tl											
Pb	36	31	36	37	52	36	46	3	6	2	7
Th	30	30	30	31	36	36	33	4	1	2	16
U	12	11	10	11	12	11	11	1	43	1	6

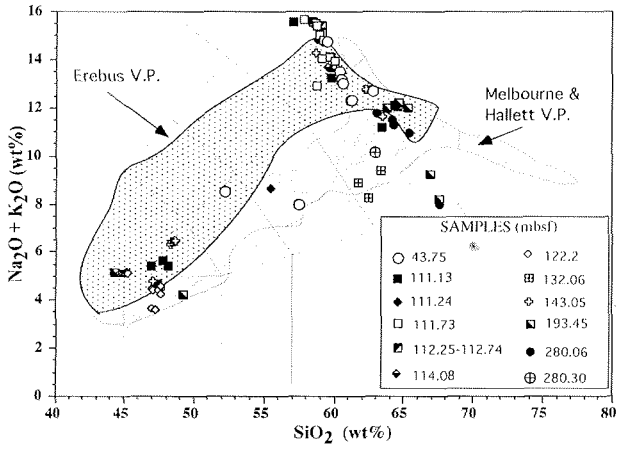

Fig. 2 - Total Alkalis-Silica (TAS) classification diagram for glass fragments found in CRP-2/2A. Composition of fields for the Erebus (South Victoria Land) and Melbourne and Hallett Volcanic provinces also shown. The dashed line separates the fields of alkaline and sub-alkaline compositions (Irvine & Baragar, 1971). Sources of data: Sun & Hanson (1975); Sun & Hanson (1976) Kyle (1990), Armienti et al.(1991) Armienti & Tripodo (1991).

the Erebus volcanic province (Mt Erebus and Minna Bluff; Wright & Kyle, 1990; Moore & Kyle, 1990). At least part of the negative linear correlation observed in the data for evolved lavas may be due to alkali loss during analysis. This is particularly true for the pumice fragments of unit 7.2, for which bulk rock conventional ICP-MS analyses (WR in the label of Tab. 3) and Laser Ablation ICP-MS data on glass shards, document a limited variability of incompatible trace elements and practically constant incompatible trace element ratios. REE patterns of the analysed samples (Fig. 3) largely overlap the compositional variability of the McMurdo Volcanic Group, with the phonolitic tephra reaching slightly higher enrichments accompanied by a more pronounced Eu anomaly (Eu/Eu* ~ 0.15). Figure 3 also shows the REE pattern of tephra fragments from the layer at 116.65 mbsf of CRP-1: both the lower REE content and different Eu anomaly (Eu/Eu* ~ 0.60) exclude any correlation between the tephras found at similar depths in CRP-1 and CRP-2/2A. The low total REE content of the alkali basalt sample from 122.22 mbsf (Fig. 3, Tab. 3) seems to be due to analytical problems more than representing a distinctive composition; major elements and La_n/Yb_n ratio (6.8), are similar to other alkali basaltic rocks of the McMurdo Volcanic Group.

MINERAL CHEMISTRY OF DIAGNOSTIC PHASES

Minerals that are more diagnostic of the occurrence of alkaline volcanism in the Ross Sea sediments are those linked to the peralkaline

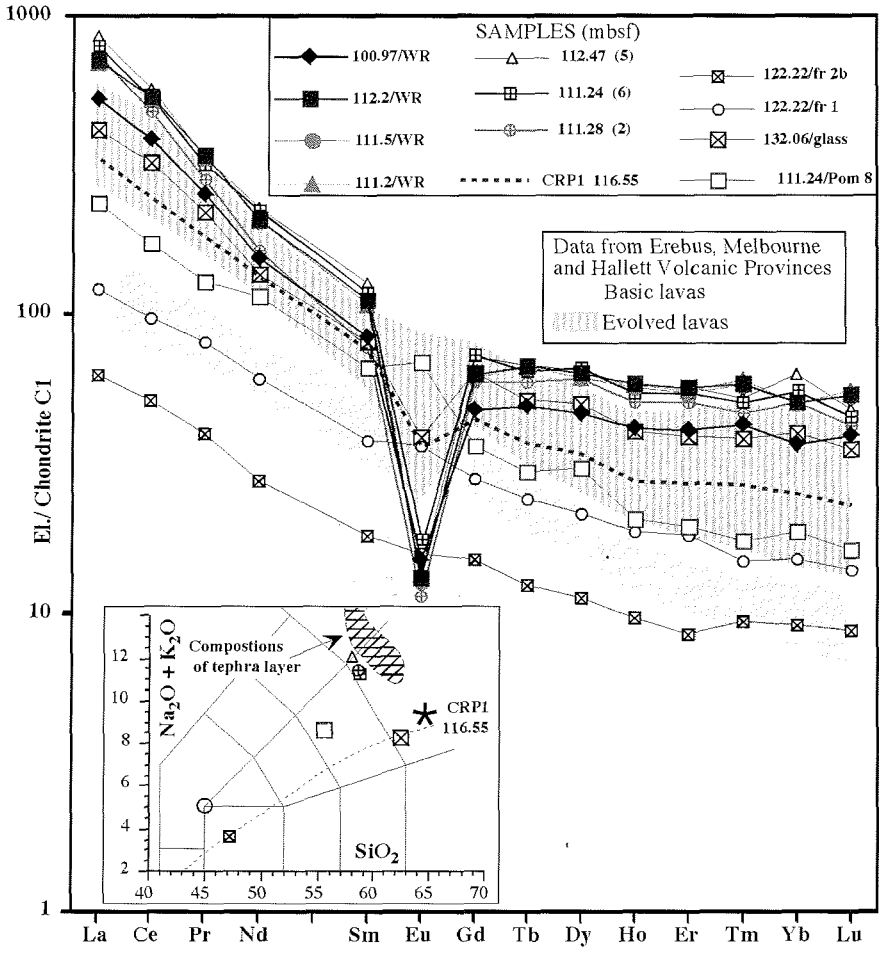

Fig. 3 - REE patterns of selected glass grains. Patterns perfectly match the known basic and evolved lavas of MVG here represented by the values of rocks from Melbourne, Hallett and Erebus Volcanic Provinces. The strongly fractionated phonolitic rocks from Mt. Erebus are excluded from the data set, due to their unusual enrichments in Lu, Eu, Tb and depletion in La and Sm, that have not been observed in the analysed glass fragments. Dashed line is the REE pattern of CRP-1 tephra at 116.55 mbsf. Normalisation is respect to C1 chondrite (McDonough & Sun, 1995). Sources of data: see figure 2. The inset reports the position in the TAS diagram of mean compositions of tephra layers. The composition of a tephra found in CRP 1 at 116.55 mbsf is also reported for comparison.

Tab. 4 - Selected SEM-EDS analyses of major elements for pyroxenes from above and below 300 mbsf. Atomic formula recast on the basis of 4 cations and 6 oxygens. Classification according to Morimoto (1988).

Depth	43.75	43.75	111.13	111.13	112.25	112.25	114.08	132.06	193.45	280.30	280.30	280.30	297.54	297.54	297.54	297.54
SiO_2	52.03	47.93	50.97	53.15	49.13	45.53	50.14	50.18	55.94	52.05	51.46	50.96	52.70	50.01	52.73	53.85
TiO_2	0.50	1.73	1.17	2.01		0.00	0.82	1.05		0.08	0.24	0.67	0.26	0.44	0.07	0.00
Al_2O_3	1.96	7.23	1.86	0.94	2.19	2.75	2.30	4.40	1.15	0.38	0.65	1.39	1.70	0.64	1.03	1.32
FeO	11.94	4.79	11.94	25.98	25.36	40.41	12.22	5.16	11.69	26.51	25.32	14.51	9.94	28.53	21.44	15.64
MnO	0.34	0.00	0.81	1.21	1.83	1.87	0.79	0.30		0.68	0.40	0.42	0.28	0.98	0.63	0.24
MgO	14.81	14.28	12.58	0.24	0.80	0.67	10.89	15.73	28.02	19.75	18.11	12.22	16.98	0.36	21.22	21.84
CaO	17.74	22.18	19.84	4.99	18.61	0.52	21.81	22.32	2.49	0.69	3.31	19.64	17.52	15.32	2.41	6.39
Na_2O	0.60	0.63	0.83	11.48	2.08	8.25	0.77	0.86	0.71	0.06		0.24	0.51	3.57	0.42	0.64
Cr_2O_3	0.08	1.23					0.26				0.07		0.11	0.15	0.05	0.08
total	100.00	100.00	100.00	100.00	100.00	100.00	100.00	100.00	100.00	100.20	99.56	100.05	100.00	100.00	100.00	100.00
	Augite	Diopside	Augite	Aegirine	Hedemb.	Aeg.-augite	Diopside	Diopside	(clino) Enst.	(clino) Enst.	Pigeonite	Augite	Augite	Aeg.-augite	(clino) Enst.	Pigeonite
Structural Formula recast on the basis of 4 cations and 6 oxygens																
Site T																
Si^{4+}	1.940	1.759	1.918	1.997	1.972	1.790	1.898	1.829	1.982	1.971	1.969	1.936	1.941	2.005	1.961	1.969
Al^{3+}	0.060	0.241	0.082	0.003	0.028	0.128	0.102	0.171	0.018	0.017	0.029	0.062	0.059		0.039	0.031
Fe^{3+}						0.082				0.012	0.002	0.002				
Site M_1																
Al^{3+}	0.026	0.072	0.000	0.038	0.076		0.001	0.018	0.030				0.015	0.030	0.007	0.026
Fe^{3+}	0.048	0.083	0.077	0.688	0.113	0.839	0.103	0.157	0.037	0.028	0.015	0.044	0.063	0.206	0.057	0.048
Ti^{4+}	0.014	0.048	0.033	0.057			0.023	0.029		0.002	0.007	0.019	0.007	0.013	0.002	
Cr^{3+}	0.002	0.036					0.008				0.002		0.003	0.005	0.001	0.002
Mg^{2+}	0.823	0.761	0.706	0.013	0.048	0.039	0.615	0.796	0.933	0.970	0.976	0.692	0.912	0.022	0.933	0.924
Fe^{2+}	0.087		0.184	0.128	0.738	0.122	0.250					0.245		0.724		
Mn^{2+}				0.038	0.025											
Site M_2																
Mg^{2+}		0.020						0.058	0.546	0.146	0.057		0.021		0.244	0.268
Fe^{2+}	0.237	0.064	0.114			0.287	0.034		0.310	0.800	0.794	0.170	0.243	0.026	0.610	0.430
Mn^{2+}	0.011		0.026		0.038	0.062	0.025	0.009		0.022	0.013	0.014	0.009	0.033	0.020	0.007
Ca^{2+}	0.709	0.871	0.799	0.201	0.800	0.022	0.884	0.872	0.095	0.028	0.136	0.798	0.691	0.659	0.096	0.250
Na^{+}	0.043	0.045	0.061	0.836	0.162	0.629	0.057	0.061	0.049	0.004		0.018	0.036	0.277	0.030	0.045
Wo	37.01	48.44	41.94	18.79	45.43	1.60	46.28	46.05	4.92	1.41	6.82	40.71	35.66	39.42	4.90	12.99
En	42.99	43.40	37.01	1.26	2.72	2.87	32.16	45.16	77.05	55.95	51.90	35.25	48.10	1.29	60.05	61.80
Fs	20.00	8.17	21.05	79.95	51.85	95.54	21.56	8.80	18.03	42.64	41.28	24.05	16.24	59.29	35.05	25.21

Depth	324.93	324.93	324.93	324.93	326.29	326.29	353.67	353.67	353.67	388.34	388.34	439.27	439.27	618.19	618.19	618.19
SiO_2	53.48	52.26	53.38	51.62	49.51	51.97	50.28	50.65	50.97	53.40	50.01	53.38	48.71	54.07	52.46	49.07
TiO_2	0.29	0.47	0.11	0.46	0.77	0.35	0.63	0.32	0.32	0.19	0.50	0.24	0.69	0.10	0.43	0.84
Al_2O_3	1.51	2.35	1.14	1.67	1.52	2.08	1.35	0.84	1.26	0.93	1.97	1.73	1.60	1.26	1.85	1.39
FeO	18.11	6.54	16.06	13.62	21.42	9.63	18.01	30.34	23.70	17.65	19.99	6.36	25.03	14.39	11.78	24.73
MnO	0.40	0.31	0.58	0.54	0.49	0.47	0.52	1.00	0.30	0.28	0.52	0.23	0.71	0.50	0.36	0.52
MgO	24.53	15.12	20.92	14.34	11.38	16.52	11.62	14.95	16.24	22.12	11.94	18.82	9.06	23.80	16.52	8.46
CaO	0.99	22.25	7.16	17.12	14.30	18.40	17.02	1.16	6.84	4.74	14.49	18.60	13.67	5.13	16.04	14.48
Na_2O	0.61	0.57	0.65	0.47	0.45	0.41	0.41	0.54	0.37	0.62	0.52			0.62	0.49	0.36
Cr_2O_3	0.08	0.13		0.16	0.16	0.17	0.16	0.20	0.00	0.07	0.06	0.19	0.13	0.13	0.07	0.15
total	100.00	100.00	100.00	100.00	100.00	100.00	100.00	100.00	100.00	100.00	100.00	99.55	99.60	100.00	100.00	100.00
	(clino) Enst.	Diopside	Pigeonite	Augite	Augite	Augite	Augite	(clino) Ferros.	Pigeonite	Pigeonite	Augite	Augite	Augite	Pigeonite	Augite	Augite
Structural Formula recast on the basis of 4 cations and 6 oxygens																
Site T																
Si^{4+}	1.948	1.923	1.962	1.938	1.914	1.918	1.928	1.970	1.941	1.961	1.919	1.954	1.931	1.960	1.944	1.936
Al^{3+}	0.052	0.077	0.038	0.062	0.069	0.082	0.061	0.030	0.057	0.039	0.081	0.046	0.069	0.040	0.056	0.064
Fe^{3+}					0.017		0.011		0.002							
Site M_1																
Al^{3+}	0.012	0.025	0.011	0.012		0.008		0.009		0.001	0.008	0.029	0.006	0.013	0.025	
Fe^{3+}	0.065	0.063	0.068	0.054	0.071	0.079	0.062	0.037	0.068	0.070	0.081		0.018	0.061	0.040	0.037
Ti^{4+}	0.008	0.013	0.003	0.013	0.022	0.010	0.018	0.009	0.009	0.005	0.014	0.004	0.021	0.003	0.012	0.025
Cr^{3+}	0.002	0.004		0.005	0.005	0.005	0.005	0.006		0.002	0.002	0.006	0.004	0.004	0.002	0.005
Mg^{2+}	0.913	0.829	0.918	0.802	0.656	0.898	0.664	0.867	0.922	0.922	0.683	0.961	0.535	0.919	0.913	0.498
Fe^{2+}		0.066		0.114	0.246		0.251	0.072	0.001		0.212		0.416		0.008	0.435
Mn^{2+}																
Site M_2																
Mg^{2+}	0.419		0.228			0.011				0.289		0.069		0.367		
Fe^{2+}	0.487	0.072	0.426	0.260	0.358	0.218	0.253	0.878	0.684	0.472	0.349	0.195	0.396	0.375	0.317	0.343
Mn^{2+}	0.012	0.010	0.018	0.017	0.016	0.015	0.017	0.033	0.010	0.009	0.017	0.007	0.024	0.015	0.011	0.017
Ca^{2+}	0.039	0.877	0.282	0.689	0.592	0.727	0.700	0.048	0.279	0.186	0.595	0.729	0.580	0.199	0.637	0.612
Na^{+}	0.043	0.041	0.046	0.034	0.034	0.029	0.030	0.041	0.027	0.044	0.039			0.044	0.035	0.028
Wo	2.00	45.74	14.53	35.57	30.54	37.34	35.92	2.50	14.22	9.57	30.75	37.25	29.48	10.29	33.07	31.50
En	68.85	43.26	59.09	41.46	33.82	46.65	34.13	44.80	46.96	62.16	35.26	52.45	27.19	66.40	47.39	25.61
Fs	29.15	11.00	26.38	22.97	35.64	16.01	29.96	52.70	38.82	28.27	33.99	10.31	43.34	23.31	19.54	42.89

compositions often attained by evolved lavas of the Cenozoic cycle of activity, namely anorthoclase feldspar and Na-rich alkali pyroxene. In the following figures and tables, all analyses are divided into two groups: above and below 300 mbsf to better demonstrate the lack of minerals diagnostic of alkaline magmas at depths below 300 mbsf. Conversely the abundance of sub-calcic pyroxene in the sediments is related to the contribution from Mesozoic tholeiitic lavas (Armienti et al., 1998). Minerals analysed in lava samples and euhedral grains of feldspars and pyroxenes occurring in the sand

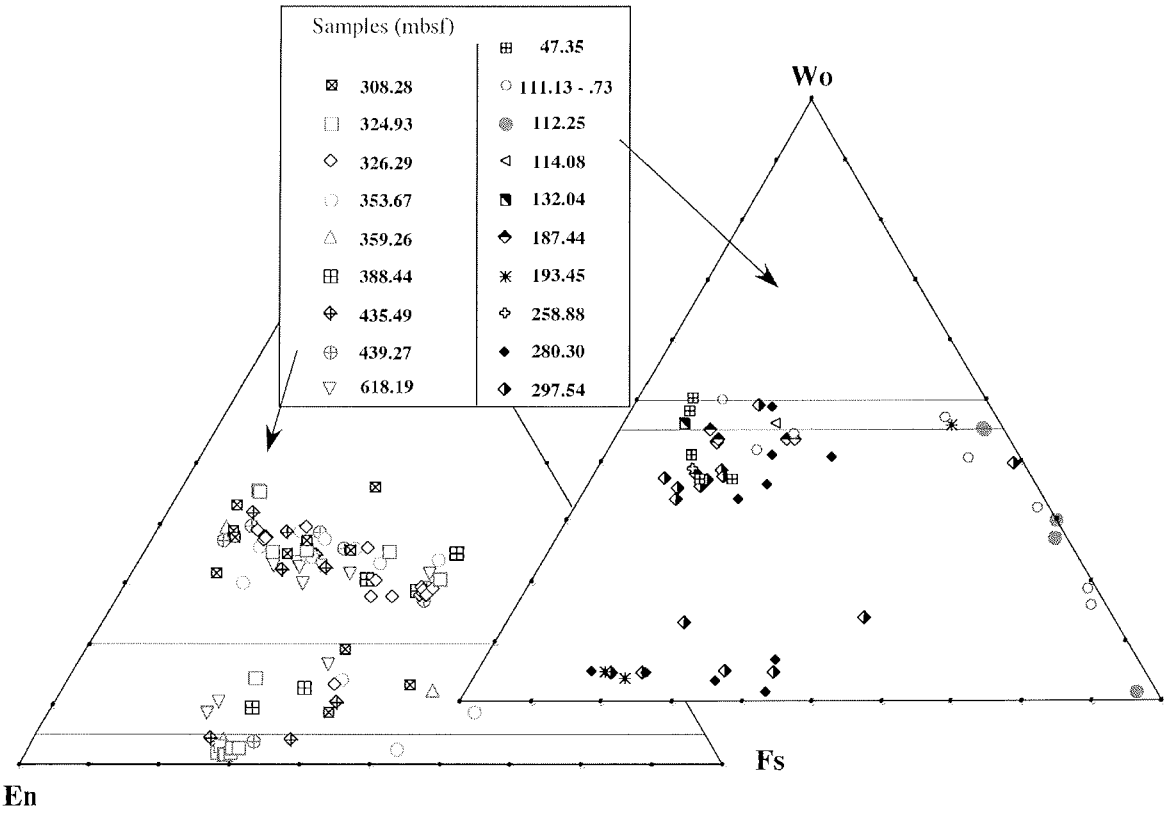

Fig. 4 - Composition of pyroxenes from CRP-2/2A samples, plotted within the Wo-En-Fs triangle. The more iron-rich augitic compositions are typical of evolved pyroxenes from peralkaline lavas, with significant amounts of a non-quadrilateral aegirine component (Morimoto, 1988).

fraction are reported in figure 4 and table 4. Aegirine-rich pyroxene, which plots next to the Wo-Fs join in the En-Wo-Fs classification diagram (Morimoto, 1988), only occurs above 300 mbsf. At depths below 300 mbsf, the lack of Na-rich pyroxene and the more pronounced development of iron enrichment in calcic pyroxenes along the calcic-subcalcic solvus, is characteristic of pyroxene crystallisation in subalkaline lavas.

Figure 5 illustrates the compositional variability of feldspar crystals above and below 300 mbsf; selected data are given in table 5. Anorthoclase compositions are never found below 300 mbsf. Above this level they occur both in volcanic clasts and tephra fragments as well as in the sand fraction as isolated grains with the typical polysynthetic twinning. They can be directly related to the input of McMurdo volcanics into the sedimentary basin along with less frequent sanidine crystals. An-rich feldspars are less diagnostic, being typical of basaltic or intermediate lavas of both tholeiitic and alkaline compositions. Or-rich feldspars are usually microcline or orthoclase derived from crystalline basement. Isolated albite grains found in samples above 300 mbsf, are probably xenocrysts sampled by explosive volcanic activity in unit 7.2, probably from altered lavas of the volcanic pile, or else derived from the crystalline basement.

Among the mafic mineral grains, numerous amphibole crystals were detected (Tab. 6). Measured compositions are dominantly iron-calcic (ferrogedrite and ferropargasite) and may be related to contributions from the crystalline basement that is dominated by hornblende-bearing granitoids (Allibone et al., 1993a, b); gedrite compositions were determined as intersertal grains in doleritic clasts (Tab. 6).

PROVENANCE CONSIDERATIONS

EVALUATION OF THE HEIGHT OF AN ERUPTIVE COLUMN RESPONSIBLE FOR THE 1.2 M-THICK TEPHRA LAYER OF UNIT 7.2

Calculations were performed to estimate the height and the distance of an eruptive column capable of dispersing pumice particles similar to those found in the 1.2 m-thick tephra fall layer of Unit 7.2, using a model of particle advection and diffusion (Armienti et al., 1988). A horizontal transport distance of 120 km was initially postulated - *i.e.* the distance to the nearest known volcanic centre on land of compatible age (Mount Morning area; Kyle 1990); particles were assumed to be of spherical shape and wind profile was considered constant with height. Two typical sizes found at the base of the layer were taken into

Tab. 5 - Selected SEM-EDS analyses of feldspars from above and below 300 mbsf.

Depth	43.75	43.75	43.75	43.75	43.75	43.75	111.13	111.13	111.13	111.13	111.13	111.73	111.73	112.25	112.25	112.25	114.08	122.22	122.22	122.22	122.22
SiO_2	48.71	63.84	56.83	65.35	66.74	64.91	52.59	54.35	57.78	64.32	65.38	65.84	63.04	66.28	63.94	60.31	62.53	47.61	53.15	51.05	55.67
Al_2O_3	32.46	23.02	25.93	19.16	18.89	20.36	29.76	28.57	26.87	19.45	20.37	19.46	22.20	19.53	21.65	25.13	23.37	33.34	29.20	29.91	27.52
Fe_2O_3	0.56		1.69	0.05	1.30	0.13	0.62	0.74		0.06	0.34	0.66	0.28	0.39			0.29	0.52	1.08	1.73	0.57
CaO	15.35	3.72	8.84	0.18	0.11	0.95	12.14	10.38	8.03	0.12	0.58	0.41	3.04	0.19	2.42	6.08	3.88	15.82	11.50	13.36	1.47
Na_2O	2.78	9.22	6.18	3.13	7.57	5.10	4.41	5.48	6.96	1.89	6.85	6.17	6.99	5.98	6.58	7.94	9.06	2.58	4.75	3.56	5.20
K_2O	0.14	0.20	0.53	12.13	5.39	8.55	0.48	0.48	0.36	14.16	6.48	7.46	4.45	7.63	5.41	0.54	0.87	0.13	0.32	0.39	9.57
Tot.	100.00	100.00	100.00	100.00	100.00	100.00	100.00	100.00	100.00	100.00	100.00	100.00	100.00	100.00	100.00	100.00	100.00	100.00	100.00	100.00	100.00
Structural formula calculated on the basis of 8 O																					
Si	2.230	2.810	2.570	2.980	2.980	2.930	2.390	2.460	2.590	2.960	2.930	2.960	2.830	2.970	2.860	2.690	2.780	2.190	2.410	2.330	2.570
Al	1.750	1.200	1.380	1.030	0.990	1.080	1.590	1.520	1.420	1.050	1.080	1.030	1.170	1.030	1.140	1.320	1.220	1.800	1.560	1.610	1.500
Fe^{3+}	0.020		0.060	0.000	0.040		0.020	0.030			0.010	0.020	0.010	0.010		0.000	0.010	0.020	0.040	0.060	0.020
Ca	0.750	0.180	0.430	0.010	0.010	0.050	0.590	0.500	0.390	0.010	0.030	0.020	0.150	0.010	0.120	0.290	0.180	0.780	0.560	0.650	0.070
Na	0.250	0.790	0.540	0.280	0.660	0.450	0.390	0.480	0.600	0.170	0.600	0.540	0.610	0.520	0.570	0.690	0.780	0.230	0.420	0.320	0.470
K	0.010	0.010	0.030	0.710	0.310	0.490	0.030	0.030	0.020	0.830	0.370	0.430	0.250	0.440	0.310	0.030	0.050	0.010	0.020	0.020	0.560
An	74.26	18.37	43.00	1.00	1.02	5.05	58.42	49.50	38.61	0.99	3.00	2.02	14.85	1.03	12.00	28.71	17.82	76.47	56.00	65.66	6.36
Ab	24.75	80.61	54.00	28.00	67.35	45.45	38.61	47.52	59.41	16.83	60.00	54.55	60.40	53.61	57.00	68.32	77.23	22.55	42.00	32.32	42.73
Or	0.99	1.02	3.00	71.00	31.63	49.49	2.97	2.97	1.98	82.18	37.00	43.43	24.75	45.36	31.00	2.97	4.95	0.98	2.00	2.02	50.91
Si+Al+Fe^{3+}	4.000	4.010	4.010	4.010	4.010	4.010	4.000	4.010	4.010	4.010	4.020	4.010	4.010	4.010	4.000	4.010	4.010	4.010	4.010	4.000	4.090
Na+K+Ca	1.010	0.980	1.000	1.000	0.980	0.990	1.010	1.010	1.010	1.010	1.000	0.990	1.010	0.970	1.000	1.010	1.010	1.020	1.000	0.990	1.100

Depth	143.05	187.44	187.44	187.44	187.44	193.45	193.45	203.86	258.88	258.88	280.06	280.06	280.06	280.30	280.30	280.30	297.54	297.54	297.54	297.54	297.54
SiO_2	64.36	59.79	59.94	50.05	57.67	58.91	53.00	64.48	52.74	49.15	61.34	65.20	54.50	55.57	47.01	65.85	52.23	46.12	64.37	63.87	64.07
Al_2O_3	19.19	23.10	24.39	31.46	26.15	25.96	29.07	19.14	29.72	32.43	24.40	18.28	28.20	27.44	33.55	17.68	29.68	33.76	19.01	19.36	19.28
Fe_2O_3	0.20	2.30	0.90	0.43	0.87		0.79	0.11	0.73	0.64			1.06		0.53	1.90	0.92	0.81	0.14	0.10	0.19
CaO		5.97	7.18	15.23	8.79	7.82	12.61	0.13	12.65	15.10	4.90		10.95	9.65	16.75	0.11	12.42	16.84	0.17	0.17	0.26
Na_2O	0.77	5.97	6.32	2.56	5.87	7.00	4.12	0.35	3.80	2.49	9.21	1.10	4.81	6.12	1.70	7.32	4.30	2.18	1.43	0.86	1.80
K_2O	15.48	2.87	1.27	0.27	0.65	0.31	0.41	15.79	0.36	0.19	0.15	15.42	0.48	0.17	0.11	5.63	0.45	0.29	14.88	15.64	14.40
Tot.	100.00	100.00	100.00	100.00	100.00	100.00	100.00	100.00	100.00	100.00	100.00	100.00	100.00	98.95	99.65	98.49	100.00	100.00	100.00	100.00	100.00
Structural formula calculated on the basis of 8 O																					
Si	2.970	2.700	2.680	2.290	2.590	2.630	2.410	2.970	2.390	2.250	2.720	3.000	2.470	2.530	2.170	2.990	2.380	2.130	2.970	2.950	2.950
Al	1.040	1.230	1.290	1.690	1.380	1.370	1.560	1.040	1.590	1.750	1.280	0.990	1.500	1.470	1.820	0.950	1.590	1.840	1.030	1.050	1.050
Fe^{3+}	0.010	0.080	0.030	0.010	0.030		0.030		0.020	0.020			0.040		0.020	0.070	0.030	0.030			0.010
Ca		0.290	0.340	0.750	0.420	0.370	0.610	0.010	0.620	0.740	0.230	0.000	0.530	0.470	0.830	0.010	0.610	0.830	0.010	0.010	0.010
Na	0.070	0.520	0.550	0.230	0.510	0.610	0.360	0.030	0.330	0.220	0.790	0.100	0.420	0.540	0.150	0.650	0.380	0.200	0.130	0.080	0.160
K	0.910	0.170	0.070	0.020	0.040	0.020	0.020	0.930	0.020	0.010	0.010	0.910	0.030	0.010	0.010	0.330	0.030	0.020	0.870	0.920	0.850
An	0.00	29.59	35.42	75.00	43.30	37.00	61.62	1.03	63.92	76.29	22.33	0.00	54.08	46.08	83.84	1.01	59.80	79.05	0.99	0.99	0.98
Ab	7.14	53.06	57.29	23.00	52.58	61.00	36.36	3.09	34.02	22.68	76.70	9.90	42.86	52.94	15.15	65.66	37.25	19.05	12.87	7.92	15.69
Or	92.86	17.35	7.29	2.00	4.12	2.00	2.02	95.88	2.06	1.03	0.97	90.10	3.06	0.98	1.01	33.33	2.94	1.90	86.14	91.09	83.33
Si+Al+Fe^{3+}	4.020	4.010	4.000	3.990	4.000	4.000	4.000	4.010	4.000	4.020	4.000	3.990	4.010	4.000	4.010	4.010	4.000	4.000	4.000	4.000	4.010
Na+K+Ca	0.980	0.980	0.960	1.000	0.970	1.000	0.990	0.970	0.970	0.970	1.030	1.010	0.980	1.020	0.990	0.990	1.020	1.050	1.010	1.010	1.020

Depth	308.28	308.28	324.93	324.93	324.93	326.29	326.29	326.29	353.87	353.87
SiO_2	55.11	63.30	45.71	53.11	55.87	58.64	63.88	50.85	63.70	46.75
Al_2O_3	28.62	18.99	35.06	29.06	27.21	25.75	19.57	30.37	19.09	33.52
Fe_2O_3	0.43	0.04		0.98	0.74	0.60	0.21	0.91	0.25	0.93
CaO	10.27	0.03	17.68	12.35	10.08	6.61	0.13	14.45	0.32	16.50
Na_2O	5.35	0.87	1.47	4.13	5.37	7.40	1.76	3.16	0.39	2.15
K_2O	0.37	15.30	0.08	0.37	0.73	1.00	14.45	0.26	16.25	0.15
Tot.	100.15	98.53	100.00	100.00	100.00	100.00	100.00	100.00	100.00	100.00
Structural formula calculated on the basis of 8 O										
Si	2.480	2.960	2.100	2.410	2.520	2.630	2.940	2.320	2.950	2.150
Al	1.520	1.050	1.900	1.560	1.450	1.360	1.060	1.640	1.040	1.820
Fe^{3+}	0.010			0.030	0.030	0.020	0.010	0.030	0.010	0.030
Ca	0.500		0.870	0.600	0.490	0.320	0.010	0.710	0.020	0.810
Na	0.470	0.080	0.130	0.360	0.470	0.640	0.160	0.280	0.040	0.190
K	0.020	0.910		0.020	0.040	0.060	0.850	0.020	0.960	0.010
An	50.51	0.00	87.00	61.22	49.00	31.37	0.98	70.30	1.96	80.20
Ab	47.47	8.08	13.00	36.73	47.00	62.75	15.69	27.72	3.92	18.81
Or	2.02	91.92	0.00	2.04	4.00	5.88	83.33	1.98	94.12	0.99
Si+Al+Fe^{3+}	4.010	4.010	4.000	4.000	4.000	4.010	4.010	3.990	4.000	4.000
Na+K+Ca	0.990	0.990	1.000	0.980	1.000	1.020	1.020	1.010	1.020	1.010

Depth	353.87	353.87	353.87	388.34	435.49	435.49	439.27	439.27	618.19	618.19
SiO_2	64.95	52.30	56.12	51.40	55.19	64.74	52.72	64.34	53.75	51.84
Al_2O_3	19.53	29.67	27.36	30.02	27.98	18.67	29.02	19.40	28.66	30.11
Fe_2O_3	0.18	0.93	0.67	0.88	0.70	0.14	1.03		0.92	0.71
CaO	0.11	12.83	9.73	13.33	10.71	0.02	12.15		11.40	13.32
Na_2O	2.27	3.91	5.68	3.96	5.05	1.15	4.57	0.76	4.81	3.75
K_2O	12.96	0.36	0.44	0.41	0.35	15.02	0.51	15.50	0.46	0.27
Tot.	100.00	100.00	100.00	100.00	99.98	99.74	100.00	100.00	100.00	100.00
Structural formula calculated on the basis of 8 O										
Si	2.970	2.380	2.530	2.350	2.490	2.990	2.400	2.960	2.440	2.360
Al	1.050	1.590	1.450	1.620	1.490	1.020	1.560	1.050	1.530	1.620
Fe^{3+}	0.010	0.030	0.020	0.030	0.020	0.010	0.040		0.030	0.020
Ca	0.010	0.630	0.470	0.650	0.520		0.590	0.000	0.550	0.650
Na	0.200	0.340	0.500	0.350	0.440	0.100	0.400	0.070	0.420	0.330
K	0.750	0.020	0.030	0.020	0.020	0.880	0.030	0.910	0.030	0.020
An	1.04	63.64	47.00	63.73	53.06	0.00	57.84	0.00	55.00	65.00
Ab	20.83	34.34	50.00	34.31	44.90	10.20	39.22	7.14	42.00	33.00
Or	78.13	2.02	3.00	1.96	2.04	89.80	2.94	92.86	3.00	2.00
Si+Al+Fe^{3+}	4.030	4.000	4.000	4.000	4.000	4.020	4.000	4.010	4.000	4.000
Na+K+Ca	0.960	0.990	1.000	1.020	0.980	0.980	1.020	0.980	1.000	1.000

Tab. 6 - Selected SEM-EDS analyses of amphiboles found as isolated grains or interstitial phases in dolerite clasts. Classification and $Fe3^+$ evaluation according to Leake et al. (1997).

Depth	43.75	111.73	111.73	112.25	112.25	280.30	326.29	326.29	326.29	326.29
SiO_2	41.50	47.98	40.13	40.07	40.51	38.18	34.74	33.60	32.95	42.98
TiO_2	1.45	0.48	1.14	1.23	0.68		2.92	1.15	1.26	1.27
Al_2O_3	9.36	6.81	10.73	9.86	10.51	22.02	16.95	18.29	18.66	11.40
FeO	30.63	20.86	28.84	31.56	30.85	33.61	28.02	31.08	30.82	21.71
MnO	1.21	0.58	1.30	1.12	1.57	1.04	0.66	0.45	0.66	0.68
MgO	2.27	9.10	2.69	1.26	1.54	5.82	10.90	13.58	12.92	7.08
CaO	10.09	12.35	10.02	10.29	9.86	1.14	0.30	0.55	0.46	12.05
Na_2O	2.40	1.15	3.18	2.70	2.47		0.43	0.33	0.37	1.29
K_2O	1.09	0.69	1.84	1.91	2.01		4.97	0.91	1.80	1.54
total	100.00	100.00	99.87	100.00	100.00	101.81	99.89	99.94	99.90	100.00
	ferro-edenite	ferrohornblende	ferropargasite	ferropargasite	ferropargasite	ferrogedrite	ferrogedrite	gedrite	gedrite	ferropargasite
Structural Formula calculated on the basis of 23 cations										
Site T										
Si^{4+}	6.503	7.109	6.327	6.394	6.408	5.559	5.323	4.878	4.830	6.462
Al^{3+}	1.497	0.891	1.673	1.606	1.592	2.441	2.677	3.122	3.170	1.538
Site C										
Al^{3+}	0.232	0.298	0.321	0.248	0.367	1.338	0.385	0.008	0.054	0.481
Fe^{3+}	0.374	0.068	0.226	0.204	0.355	1.102	0.647	2.630	2.502	0.162
Ti^{4+}	0.171	0.053	0.135	0.148	0.081		0.336	0.126	0.139	0.144
Mg^{2+}	0.530	2.010	0.632	0.300	0.363	1.263	2.490	2.237	2.306	1.587
Fe^{2+}	3.640	2.517	3.577	4.007	3.726	1.296	1.142			2.568
Mn^{2+}	0.053	0.054	0.109	0.093	0.108					0.059
Site B										
Mg^{2+}								0.702	0.517	
Fe^{2+}						1.694	1.801	1.143	1.276	
Mn^{2+}	0.107	0.018	0.064	0.058	0.102	0.128	0.086	0.055	0.082	0.027
Ca^{2+}	1.694	1.960	1.693	1.759	1.671	0.178	0.049	0.086	0.072	1.941
Na^+	0.199	0.021	0.243	0.183	0.227		0.064	0.014	0.052	0.032
Site A										
Na^+	0.531	0.309	0.729	0.653	0.530		0.064	0.079	0.053	0.344
K^+	0.218	0.130	0.370	0.389	0.406		0.972	0.169	0.337	0.295
$Mg/(Mg+Fe^{2+})$	0.127	0.444	0.150	0.070	0.089	0.297	0.458	0.720	0.689	0.382

account: 1 mm and 2 mm; computations were performed for particle densities of 1.0 and 2.5 gcm^{-3}. Resulting settling velocities (Vs) are in the range 4.43-11.04 ms^{-1} . The results of the calculations are shown in figure 6, where the heights of release of the different classes of particles from an eruptive column, are plotted as a function of the wind speed required to travel a given distance D. Additional computations were also performed for 6 mm particles with a density of 1.0 gcm^{-3} (Vs=12.9 ms^{-1}) and for a travel distance of 30 km, for which column height estimates provide values below 25 km for wind speeds larger than 50 km/h (Fig. 6, curve #5). Even if larger particles may have floated and travelled before sinking to the sea floor, unrealistic column heights or wind speeds would be required for immediate deposition by fallout for an assumed distance of 120 km from the source (Fig. 6, curve #1), the occurrence of smaller and more dense particles (curve #2) allow to reach the same conclusion. For 2 mm pumices with density of 1.0 gcm^{-3} (Fig. 6, curves #3 and #6), a crude estimate of column height, for a distance between 30 and 120 km and wind speed of 100 km/h is between 33 and 8 km. Note that a high wind speed would determine deposition of tephra only in a narrow, strongly elongated region along the dispersal axis, thus reducing the probability of sampling the deposit. Even if some transport of floating pumice on the sea surface seems to be implied by the rounded shape of the pumice fragments, the direct fall of particles of about 6 mm of diameter in the bulk of the layer suggests that a column not higher than about 12 km was responsible of the deposition of the tephra (Fig. 6, curve #5) for a wind speed of 100 km/h. This implies that the volcanic source may have been closer than 30 km, and suggests the occurrence of an unknown volcanic centre, possibly within 30 km of Cape Roberts. The prominent magnetic anomalies identified in the Ross Sea, north of the drilling site (Behrendt, 1990), are tentatively suggested as possible volcanic sources that were subaerially exposed at the time of the eruption.

IMPLICATIONS OF VOLCANIC DETRITUS IN CRP-2/2A CORE

Glass and volcanic rock fragments together with peralkaline minerals clearly related to MVG alkaline volcanic activity are recorded in CRP-2/2A sediments only above about 300 mbsf. Their large chemical and petrographic variability (Fig. 2, Tab. 1), suggests that a variety of volcanic sources were contemporaneously supplying sedimentation in the basin. Alkali-rich pumices of phonolitic composition characterise the tephra layers in Unit 7.2: even if they do not reach the enrichment of incompatible elements found in some recent Mt. Erebus phonolites, they are among the most evolved rocks ever found in the McMurdo

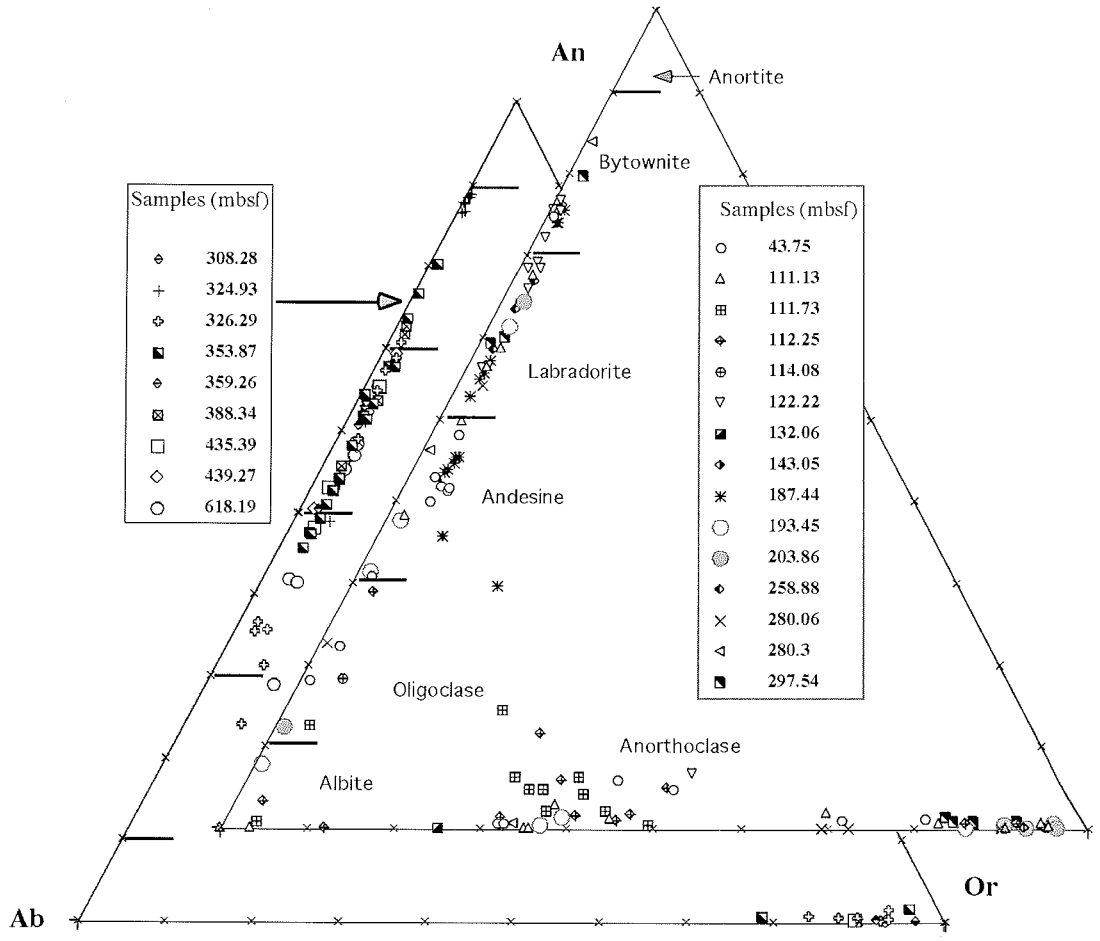

Fig. 5 - Compositions of feldspars from CRP-2/2A samples. Anorthoclase feldspar commonly occurs along with aegirine-augite, suggesting a common source from peralkaline volcanics of the MVG. Microcline, orthoclase and oligoclase are commonly present in polycrystalline aggregates within the crystalline basement. Albitic feldspars found in samples above 300 mbsf are isolated crystals in unit 7.2, probably xenocrysts sampled by explosive activity and derived from altered lavas or from the crystalline basement.

Volcanic Group (Fig. 3). This suggests the occurrence of strato-volcanoes fed by magma chambers in which differentiation process could take place. Their position is presently unknown, since the considerations about the eruptive column, discussed above, seem to rule out a provenance from the coeval volcanic centre at Mount Morning. Evolved rocks of alkaline composition characterise the volcanic detritus since its early appearance in the sedimentary record (Fig. 2), suggesting that the occurrence of differentiation processes distinguishes magmatic activity of McMurdo Volcanic Group, since its onset, in south Victoria Land. The abundance of fine grains of volcanic origin in most sandstone layers above 300 mbsf, implies that in addition to glaciers, a dominant role for wind transport from exposed volcanic rocks is to be invoked. Below 300 mbsf dolerite and unvesiculated basalt fragments of tholeiitic affinity are the only volcanic constituents present. In this part of the core they are more abundant than crystalline basement clasts, moreover the widespread occurrence of sub-calcic pyroxene

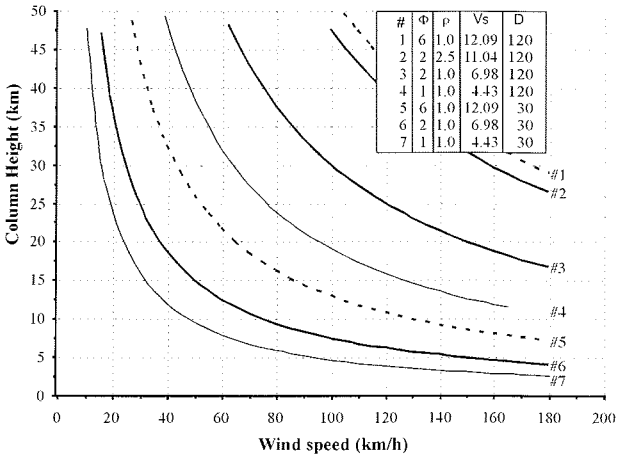

Fig. 6 - For pumice particles of 1, 2 and 6 mm of diameter and different densities (properties affecting settling velocity in air), the curves show the height of release (y axis) required, for a given wind speed (x axis) in order to make particles fall at a distance of 120 and 30 km. Unrealistic heights of release (>30 km) or wind speeds >>100 km/h are required to explain the occurrence of larger pumices in the tephra layer. See text for further explanation. ϕ - particle diameter (mm); ρ - particle density (gcm^{-3}); V_S - particle settling velocity ($msec^{-1}$); D - assumed travel distance (km).

grains in the sand matrix, and the amount of rounded quartz grains reworked from Beacon sandstone units (Smellie, 2000; Talarico et al., 2000) suggest for them a source related to erosion of the sedimentary and volcanic sequences overlaying the crystalline basement. Armienti et al. (1998) report, for the nearby CRP-1 drill site, distinctive horizons that are typically enriched in volcanics: the basalt glass-rich layer at 43.62 mbsf, the levels at about 61 mbsf and at 116.55 mbsf. The last two levels were dated by McIntosh (1998) at 18.12-17.30 and 18.4 Ma, respectively. None of these levels was recognised in CRP-2/2A. In fact, in CRP-2/2A, no Cenozoic sandstone is so distinctively enriched in basaltic glass as CRP-1 43.62 mbsf, and the tephra CRP-1 116.55 mbsf, a possible stratigraphic marker, does not match in age and composition (Fig. 3, inset) the tephra of unit 7.2 of CRP-2/2A.

CONCLUSIONS

MVG-derived glass, volcanic rock fragments and peralkaline minerals clearly related to alkaline volcanic activity are recorded in CRP-2/2A sediments only above about 300 mbsf (Unit 9.8). The presence of $^{40}Ar/^{39}Ar$ dated peralkaline trachyte tephra at 280.06 mbsf indicates that rift-related magmatic activity in south Victoria Land commenced at 24.22 ± 0.06 Ma (latest Oligocene) at a much later time (about 24 Myr younger) relative to the alkaline volcanism in the northern part of the Ross Sea rift system (*cf.* Tonarini et al., 1997). Volcanic detritus above 300 mbsf, appears to be derived from a variety of volcanic sources and, in addition to glaciers, a dominant role for wind transport from exposed volcanic rocks is inferred as for CRP-1. Below 300 mbsf dolerite and basalt fragments of tholeiitic affinity are the only volcanic constituents present. Their greater abundance with respect to crystalline basement clasts, the widespread occurrence of sub-calcic pyroxene grains in the sand matrix, and the amount of rounded quartz grains reworked from Beacon sandstone units suggest a source related to erosion of the sedimentary and igneous sequences resting on the crystalline basement. In this context the occurrence of an intraformational breccia between 324 and 320 mbsf could be a sedimentary response to coeval tectonic instability accompanying the uplift of the Transantarctic Mountains and preceding the onset of Cenozoic volcanism. Distinctive horizons in CRP-1 (*e.g.* the basalt glass-rich layer at 43.62 mbsf and trachytic tephra-bearing layers at 60 mbsf and 116.55 mbsf (Armienti et al., 1998) were not recognised in CRP-2/2A. This limits the use as regional stratigraphic markers of tephra layers deposited adjacent to advancing and retreating glaciers.

ACKNOWLEDGEMENTS - This work has been performed with the financial support of Italian *Programma Nazionale di Ricerche in Antartide* (PNRA). A special thank to Dr. P. Bottazzi (*Centro per la Cristallochimica e Cristallografia*, Pavia, Italy) for the help in the LAMS chemical Analyses, and to Dr. Massimo D'Orazio (*Dipartimento di Scienze della Terra, Università di Pisa*), for the assistance in ICP chemical analyses. This work benefited of the fruitful discussions with Dr. John Smellie of the British Antarctic Survey and of his careful revision.

REFERENCES

Allibone A.H., Cox S.C., Graham I.J., Smillie R.W., Johnstone R.D., Ellery S.G. & Palmer K., 1993a. Granitoids of the Dry Valleys area, southern Victoria Land, Antarctica: plutons, field relationships and isotopic dating. *N. Zeal. J. Geol. Geophys.*, **36**, 281-297.

Allibone A.H., Cox S.C..& Smillie R.W., 1993b. Granitoids of the Dry Valleys area, southern Victoria Land, Antarctica: Geochemistry and evolution along the early Palaeozoic Antarctic Craton margin. *N. Zeal. J. Geol. Geophys.* , **36**, 299-316.

Armienti P. & Tripodo A., 1991. Petrography and chemistry of lavas and comagmatic xenoliths of Mt. Rittmann, a volcano discovered during the IV Italian expedition in Northern Victoria Land (Antarctica). *Mem. Soc. Geol. It.*, **46**, 427-451.

Armienti P., Civetta L., Innocenti F., Tripodo A., Villari L.& Vita G., 1991. New petrological and geochemical data on Mt. Melbourne volcanic field, Northern Victoria Land, Antarctica. *Mem. Soc. Geol. It.*, **46**, 397-424.

Armienti P., Macedonio G.& Pareschi M.T., 1988. A numerical model for the simulation of tephra transport and deposition: applications to May 18, 1980 Mt. St. Helens eruption. *J. Geoph. Res.*, **93**, 6463-6476.

Armienti P., Messiga B. & Vannucci R., 1998. Sand provenance from major and trace element analyses of bulk rock and sand grains. *Terra Antartica*, **5**, 589-599.

Balestrieri M.L., Bigazzi G. & Ghezzo C., 1997. Uplift-denudation in the Transantarctic Mountains between the David and Mariner glaciers, northern Victoria Land (Antarctica): constraints by apatite fission-track analysis. In: Ricci C.A.(ed.), *The Antarctic Region: Geological evolution and processes*, Terra Antartica Publication, Siena, 547-554.

Behrendt J.C., 1990. A.12 Ross Sea. In: LeMasurier W.E. & Thomson J.W. (eds.), *Volcanoes of the Antarctic Plate and Southern Oceans*, American Geophysical Union, Antarctic Research Series, **48**, 89-90.

Cape Roberts Science Team, 1998. Quaternary Strata in CRP-1, Cape Roberts Project, Antarctica, *Terra Antartica*, **5**, 31-61.

Cape Roberts Science Team, 1999. 4-Petrology, Studies from the Cape Roberts Project, Ross Sea Antarctica. Initial report on CRP2/2A, *Terra Antartica*, **6**, 89-106.

Diester-Haass L., Robert C., & Chamley H., 1996. The Eocene-Oligocene transition in the Atlantic sector of the Southern Ocean (ODP Site 690), *Marine Geology*, **131**, 123-149.

Duncumb P. & Reed S.J.B., 1968. Quantitative Electron Probe Microanalysis. In: Heinrich K.F.J. (ed.). *NBS Spec Pub.* **298**, 133pp.

Ehrmann, W.U. & Mackensen A., 1992. Sedimentological evidence for the formation of an East Antarctic Ice Sheet in Eocene/Oligocene time. *Palaeogeogr. Palaeoclimatol. Palaeoecol.* , **93**, 85-112.

Irvine T.N. & Baragar W.R.A., 1971. A guide to the chemical classification of the common volcanic rocks. *Canad. J. Earth Sci.*, **8**, 523-548.

Jackson S.E., Longerich H.P., Dunning G.R.& Fryer B.J., 1992. The application of laser-ablation microprobe-inductively coupled plasma-mass spectrometry (LAM-ICP-MS) to in situ trace-element determination in minerals. *The Canadian Mineralogist*, **30**, 1049-1064.

Kyle P.R., 1990. McMurdo Volcanic Group, western Ross embayment. In: LeMasurier W.E. & Thomson J.W. (eds.),

Volcanoes of the Antarctic Plate and Southern Oceans. American Geophysical Union, Antarctic Research Series, **48**, 19-25.

Leake B.E, Woolley A.R., Arps C.E.S, Birch W. D., Gilbert M., Grice J.D., Hawthorne F. C., Kato A., Kisch H.J., Krivovichev V.G., Linthout K., Laird J.; Mandarino J.A., Maresch W.V., Nickel E.H., Rock N.M.S., Schumacher J.C., Smith D.C., Stephenson N.C.N., Ungaretti L., Whittaker E.J.W. & Guo Y., 1997. Nomenclature of amphiboles; report of the subcommittee on amphiboles of the International Mineralogical Association, Commission on New Minerals and Mineral Names. *The Canadian Mineralogist*, **35**, 219-246.

Leoni L., Sbrana A. & Tamponi M., 1989. La microanalisi con il Microscopio Elettronico a Scansione. Il sistema EDAX PV 9900 ed il metodo SUPQ. *Atti Soc. Tosc. Sci. Nat.*, A **96**, 193-204.

McDonough, W.F. & Sun. S.-S., 1995. The composition of the Earth. *Chem. Geol.*, **120**, 223-253.

McIntosh W.C., 1998. $^{40}Ar/^{39}Ar$ geochronology of volcanic clasts and pumice in CRP-1 core, Cape Roberts, Antarctica. *Terra Antartica*, **5**, 683-690.

Moore J.A. & Kyle P.R., 1990. A.17. Mt Erebus. In: LeMasurier W.E. & Thomson J.W. (eds.), *Volcanoes of the Antarctic Plate and Southern Oceans*. American Geophysical Union, Antarctic Research Series, **48**, 103-108.

Morimoto N., 1988. Nomenclature of Pyroxenes. *Mineralogy and Petrology*, **39**, 55-76.

Philibert A., 1963. Proc. III Int. Symp. X-Ray and X-Ray Microanalysis. Stanford University. Pattee H.H., Cosslett V.E. & Engstrom A. (eds.), Academic Press. New York. 379 p.

Smellie J.L., 1998. Sand Grain Detrital Modes in CRP-1: provenance variations and influence of Miocene eruptions on the marine record in the McMurdo Sound region. *Terra Antartica*, **5**, 579-587.

Smellie J.L., 2000. Erosional History of the Transantarctic Mountains Deduced from Sand Grain Detrital Modes in CRP-2/2A, Victoria Land Basin, Antarctica. *Terra Antartica*, **7**, 545-552.

Sun S.S. & Hanson G.N., 1975. Origin of Ross Island basanitoids and limitation upon the etherogeneity of mantle sources for alkali basalts and nephelinites. *Contrib. Mineral. Petrol.*, **52**, 77-106.

Sun S.S. & Hanson G.N., 1976. Rare earth evidences of differentiation of McMurdo volcanics, Ross Island, Antarctica. *Contrib. Mineral. Petrol.*, **54**, 139-155.

Talarico F., Sandroni S., Fielding C. & Atkins C., 2000. Variability, petrography and provenance of basement clasts in core from CRP-2/2A, Victoria Land Basin, Antarctica. *Terra Antartica*, **7**, 529-544.

Tonarini, S., Rocchi, S., Armienti, P. & Innocenti, F., 1997. Constraints on timing of Ross Sea rifting inferred from Cainozoic intrusions from northern Victoria Land, Antarctica. In: Ricci, C.A. (ed.), *The Antarctic Region: Geological evolution and processes*. Terra Autartica Publication, Siena, 511-521.

Wright A.C. & Kyle P.R., 1990. A.20 Minna Bluff. In: LeMasurier W.E. & Thomson J.W. (eds.), *Volcanoes of the Antarctic Plate and Southern Oceans*, American Geophysical Union, Antarctic Research Series, **48**, 117-119.